Journal of Anatomy

J. Anat. (2009) **214**, pp374–387 doi: 10.1111/j.1469-7580.2008.01040.x

3D representation of the developing chick knee joint: a novel approach integrating multiple components

Karen A. Roddy,[1,2] Niamh C. Nowlan,[1,2] Patrick J. Prendergast[2] and Paula Murphy[1]

[1]*Department of Zoology, School of Natural Sciences, Trinity College, Dublin, Ireland*
[2]*Trinity Centre for Bioengineering, School of Engineering, Trinity College, Dublin, Ireland*

Abstract

The knee joint has a highly complex 3-dimensional (3D) morphology that is sculpted at the interface of the forming long bones as they are generated in the embryo. Although it is clear that regulatory genes guide joint formation, the mechanisms that are responsible for morphogenesis of the knee are poorly understood. Certainly the process involves integration across several tissues and physical/mechanical influences from neighbouring tissues are important. We describe the acquisition of shape in the chick knee joint in detail and show that by HH34 the joint already displays shape characteristics of the adult structure. Through imaging developing cartilage, tendons, ligaments and muscle across developmental stages from HH28–34 we have built 3D representations of the forming structure including the various components important in knee formation. We describe the timing of muscle and tendon development in parallel with the refinement of cartilage shape, showing when and where (tendon attachment points) muscle forces are applied to the cartilage elements. Shape begins to emerge as the tendons are forming (HH30–32) but is fully refined (HH34) in the presence of tendons. The resulting integrated 3D representations of the developing knee across time will serve as the foundation for computational analysis of the mechanical environment, and experimental approaches to investigating morphogenetic mechanisms.

Key words 3D imaging; cartilage template; computer model (representation); joint capsule; knee joint; marker gene expression; morphogenesis; muscle masses; tendon attachment points.

Introduction

Joint morphogenesis is a vital phase in skeletogenesis involving the co-ordinated development of several elements of the musculoskeletal system. Previous studies have focused on the development of individual elements such as the cartilage template (Fell, 1925; Mitrovic, 1977; Bi et al. 1999; Hartmann & Tabin, 2000), muscles and tendons (Shellswell & Wolpert, 1977; Kardon, 1998; Benjamin & Ralphs, 2000; Schweitzer et al. 2001; Buckingham et al. 2003) and the joint capsule (Mitrovic, 1978; Nalin et al. 1995; Bland & Ashhurst, 1997). However, failure to create or maintain correct co-ordination between constituent tissues during gestation leads to abnormalities (Rodriguez et al. 1988; Kardon, 1998; Garciadiego-Cazares et al. 2004). An improved anatomical description of the emerging joint structure would allow a more complete investigation of the regulatory relationships between constituent elements.

This paper presents an integrated picture of the emerging knee joint region within a defined developmental period in which many key structures of the musculoskeletal system are clearly defined (HH28–HH34 focusing mainly on stages HH30, HH32 and HH34). The use of the 3D imaging technique optical projection tomography (OPT) (Sharpe et al. 2002) facilitated this work in allowing capture of the distribution of tissue specific markers, either colourimetrically or fluorescently visualized, within a 3D morphological context. OPT has recently been used for 3D recording and representation of late stage mouse limb morphogenesis (DeLaurier et al. 2006), adult mouse pancreatic tissues (Alanentalo et al. 2007) and plant development (Lee et al. 2006), in addition to its wider use to record gene expression patterns (Kerwin et al. 2004; Sarma et al. 2005; Borello et al. 2006; Lioubinski et al. 2006; Miller et al. 2007; Summerhurst et al. 2008). Once captured, data can be represented in several different ways including external views of the whole specimen, surface representations to view the outline of a structure or labelled tissue, or virtual sections through the specimen in any orientation. These techniques are used here to build 3D computer representations of the developing chick knee joint illustrating the close temporal and spatial relationship between the forming cartilage, tendon, muscle, joint capsule and synovial cavity. While the development of individual tissues has been described in previous papers, the focus of this work is to

Correspondence
Dr Paula Murphy, Department of Zoology, Trinity College Dublin, Ireland, T: + 353 1 8963780; F: + 353 1 6778094; E: paula.murphy@tcd.ie

Accepted for publication *25 November 2008*

Table 1 Details of cDNA clones used as probes for expression analysis

Marker gene	ChEST ref	Extent of probe on GenBank sequence (accession no.)
Scleraxis	ChEST654f15	Nucleotide 416–1109 on **NM_204255.1**
α1 Collagen type XI	ChEST66f22	Nucleotide 1826–2496 on **NM_88593.1**

integrate events in a set of 3D models of the emerging joint; models that will be useful as a basis and frame of reference for both computational and experimental manipulation of the system to investigate morphogenetic mechanisms. Computational methods such as finite element analysis that reveal mechanical influences acting on the forming structure will benefit from the realistic morphologies generated using this approach (Nowlan et al. 2008). The 3D detail represented in the models will facilitate comparisons with experimental situations to reveal subtle changes in morphology or timing of events; for example following physical alterations such as immobilization or surgery (e.g. Lelkes, 1958; Drachman & Sokoloff, 1966; Osborne et al. 2002) and genetic alteration of regulatory molecules. We propose to create a spatial and temporal dataset for joint morphogenesis in three dimensions, where precise shapes and precise locations of tendon attachment points are represented digitally, that can be used to definitively test theories about regulation of joint formation.

Materials and methods

Embryo collection

Fertilized chick eggs, supplied by Enfield broiler breeders (breed: Ross 308) were incubated (Natureform UT350N) at 37 °C with 70% humidity for 6–9 days. The collected embryos were staged using Hamburger and Hamilton (HH) criteria (Hamburger & Hamilton, 1951).

Alcian blue staining

Left hind limbs of stage HH28–HH34 chick embryos were dissected and fixed in 95% ethanol for 3 days. The limbs were then stained using a modification (0.1% Alcian blue instead of 0.015%) of the protocol described by Hogan et al. (1994) for 8 h and washed twice in 95% ethanol. The limbs were subsequently cleared in 1% potassium hydroxide and fixed in 4% paraformaldehyde (PFA) in phosphate-buffered saline (PBS) at 4 °C overnight. At least 10 specimens per stage were stained and at least five specimens per stage analysed using OPT.

Whole-mount *in situ* hybridization

Probe preparation

Several collagen types, including collagen type XI have been used previously as markers of the joint capsule and the forming patella (Craig et al. 1987; Nalin et al. 1995; Bland & Ashhurst, 1997). Collagen type XI is formed from heterotrimers composed of α1 (XI), α2 (XI) and α3 (XI) chains (reviewed in Eyre, 2002; Gelse et al. 2003). The α1 (XI) gene transcript was used as a marker in this study. The BBSRC ChickEST Database and its associated bank of expressed sequence tags (ESTs) (Boardman et al. 2002) provided cDNA clones for the genes *α1 Collagen type XI* and *Scleraxis*. The database was searched for ESTs located within the genes of interest and two ESTs were then selected. The ESTs were chosen based on the quality of alignment (Chenna et al. 2003) and position within the gene, with ESTs of 0.5–1.0 kb preferred. Details of the probes used are shown in Table 1. Antisense and sense digoxigenin-labelled RNA probes were generated from appropriately linearized plasmid DNA, using T7 and T3 promoter sites in the pBluescript II KS+ vector (all reaction components from Roche, Germany). The probes were purified on G25 columns (Amersham biosciences, USA) as per manufacturer's instructions.

Fixation and hybridization

After dissection, right hind limbs of HH30, 32 and 34 chick embryos were fixed in 4% PFA overnight and *in situ* hybridized largely as per Xu & Wilkinson (1998) with the following changes. The limbs were permeabilized by treatment with 20 μg mL^{-1} proteinase K in PBT (PBS + 0.1% TritonX100) for 1 min per embryonic stage (e.g. 32 min for stage HH32). At least 10 embryos (individual right hind limbs) at each stage were hybridized in at least two independent hybridizations. The limbs were hybridized with 1 μg mL^{-1} of digoxigenin-labelled labeled probe for 3 nights (65 °C). Hybridization with sense probe was used as a negative control (3 specimens per duplicate experiment). After hybridization the un-hybridized probe was removed by washing twice in 2× SSC for 10 min, three 20-min washes in 2× SSC/0.1% 3-[(3-cholamidopropyl) dimethylammonio]-2-hydroxy-1-propanesulfonate (CHAPS) and three washes for 20 min in 0.2% SSC/0.1% CHAPS, all at 65 °C. This was followed by two 10-min washes in 0.1 M Tris pH 7.5/0.15 M NaCl/1% Tween 20 at room temperature. The embryos were subsequently washed for 2–3 h in blocking solution (3% blocking powder in maleic acid buffer). The limbs were incubated overnight at 4 °C with 1/1000 dilution of anti-digoxigenin Fab fragments conjugated with alkaline phosphatase (Roche, Germany) in fresh blocking solution. For larger specimens the chromogenic reaction was developed at 4 °C with half strength stain to aid in penetration. The resulting stained limbs were photographed using an Olympus SZX12 with attached camera (Qimaging micropublisher 3.3). At least four specimens (two per duplicate experiment) representative of the externally visible pattern, were selected for OPT scanning.

Whole-mount immunohistochemistry

The myogenic cell population was visualized in this study using an anti-myosin antibody. Tendons were visualized by localization of the extracellular protein tenascin and transcripts of the bHLH transcription factor encoding gene *Scleraxis*, both previously used as tendon markers (Cserjesi et al. 1995; Kardon, 1998; Schweitzer et al. 2001; Asou et al. 2002). The right hind limbs of HH30, 32 and

34 embryos were dissected, washed in 50% methanol and fixed in Dents (1 : 4 dimethyl sulfoxide : MeOH) for 2 h. Limbs were then washed in 1 : 1 1× TBST: MeOH for 30 min, 100% TBST (25 mM Tris, 140 mM NaCl, 3 mM KCl, 0.05% Tween-20, pH 8.0) overnight and blocked overnight in 10% goat serum in TBST. Five hind limbs were analysed in each of two duplicate experiments (10 specimens). The limbs were incubated with two primary antibodies, anti-myosin mf20 IgG [1 : 20 dilution; Developmental Studies Hybridoma Bank (DSHB), Iowa City, IA, USA] and rabbit anti-tenascin IgG (1 : 500 dilution, Chemicon) in blocking solution (10% serum in 1× TBST plus 0.01% Na azide) for 5 days at 4 °C and washed a minimum of four times and once overnight with 1× TBST. Two further washes in 1× TBST (1 h) were followed by a further two in blocking solution. Limbs were then incubated with secondary antibodies (Alexa Fluor 528 goat anti-mouse IgG and Alexa Fluor 488 goat anti-rabbit IgG, Molecular Probes, 1 : 200 dilution) in fresh blocking solution overnight and washed in 1× TBST. Controls (three specimens in each duplicate experiment) were exposed to only secondary antibodies.

Preparation and imaging of embryonic limbs using OPT

The specimens were embedded in 1% agarose and scanned as per Summerhurst et al. (2008). At least two scans were performed for each specimen using UV light and a TXR filter (560/40 nm excitation, 610LP nm emission), a GFP1 filter (425/60 nm excitation, 480 nm emission) or a GFP2 filter (480/40 nm excitation, 510 nm) and, for colourimetric staining, the data were imaged using visible light and a 700-nm or 750-nm filter for very intense staining. Autofluorescence from the tissue was captured to reconstruct embryo morphology. The raw data, consisting of 400 images from each of the scans, were loaded onto a Linux workstation and reconstructed using a set of programs provided by the Edinburgh Mouse Atlas Project (EMAP) (http://genex.hgu.mrc.ac.uk/intro.html) and analysed using custom-made software (MAPAINT, MA3DView), again provided by EMAP.

Histology

The knee joint region of hind limbs of stage HH28, 30, 32 and 34 chick embryos (at least three specimens per stage) were dissected, skinned and fixed for 4 h in 4% PFA. The specimens were then washed for 30 min in 0.85% NaCl (4 °C) and dehydrated in graded solutions of ethanol (2× 1 : 1 0.85% NaCl: EtOH, 15 min; 70% EtOH, 15 min; 70% EtOH, 30 min; 90% EtOH, 1 h; 2× 100% EtOH, 1 h) followed by 1 h in Histoclear, an hour in 1 : 1 Histoclear: paraffin wax (60 °C) and two changes of wax before embedding. Serial sections of 5 μM were cut using a microtome. Slides were subsequently stained using 0.5% Alcian blue (30 min) and Harris Haematoxylin (6 min) (Sigma-Aldrich). The sections were mounted and photographed using a Nikon Optiphot-2 microscope mounted with a Canon EOS 350D camera.

The distribution of cells in the joint region was quantified on a total of three sections located 25 μM apart per specimen and three specimens per stage. For each section, cells were counted in a total area of 100 × 400 μM spanning the joint. Cell counts were carried out within a sliding window of area 100 × 40 μM which was moved 20 μM perpendicular to the joint surface following each count. If the cells within the window were definably cartilaginous in nature (round with clear Alcian blue staining) they were classified as cartilage frames. Frames containing flattened cells with minimal Alcian blue staining were classified as interzone. Those frames spanning the margin were only classified as a particular state if greater than 50% of the frame contained cells of that type.

Results

The changing shape of the cartilage elements and the forming knee joint

The development of future skeletal elements in the avian hind limb was observed and recorded in 3D using OPT at stages HH28–34 following Alcian blue staining. Here we focus on describing the morphogenesis of the knee joint, although the whole limb was imaged and development of other joints is briefly noted. The analysis is summarized in Fig. 1 showing dorsal views of 3D volume representations following computer reconstruction of stained limbs (Fig. 1a–g) and extracted surface representations of the cartilage rudiments in the knee region (Fig. 1h–n) and foot plate (Fig. 1o–u).

The joints appear in a proximal to distal order, as previously described (Mitrovic, 1978). Already at HH28, the position of the future knee, ankle and metatarsal-phalangeal-joints (MTP) of digits III and IV (Fig. 1a) were visible as a reduction in the intensity of Alcian blue staining, in the case of the knee, at the branching of the femur from the future tibiotarsus (Fig. 1h). The MTP joints of digits III and IV were more clearly defined by HH29 (Fig. 1p) and the position of the MTP joint of digit II was indicated by HH30 (Fig. 1c,q). The position of the first inter-phalangeal joints also appeared at HH30 (Fig. 1c, indicated by *) with the more distal cartilage condensations of the foot, and their associated joints, added progressively so that by HH34 (Fig. 1g2,u) a complement of four metatarsal and nine phalangeal rudiments were evident in the foot. Unlike digits II, III and IV, the metatarsal of digit I remained quite small and will not contribute to the metatarsus (Bellairs & Osmond, 2005).

Focusing on the knee, whereas a presumptive joint region was clearly indicated by a reduction in Alcian blue staining of the cartilaginous anlagen by HH28, some residual staining was present, particularly on the side of the fibula (Fig. 1a,h). Gradual loss of Alcian blue staining is a feature of joint progression during the appearance of a histologically distinct interzone. Dramatic changes can be seen in the overall shape of the cartilaginous elements as they separate across the joint line (compare Fig. 1h,n). At early stages the termini of the skeletal elements that will ultimately form the articulating surfaces of the joint, lack congruency and have a relatively simple flat shape (Fig. 1h). These undergo morphogenesis with the appearance of rounded prominences of the articulating surfaces (condyles) and protrusion of the future cranial cnemial crest during the timeframe of the study. The first shape changes are evident even before the full definition of the individual elements at HH32 (indicated by complete loss of

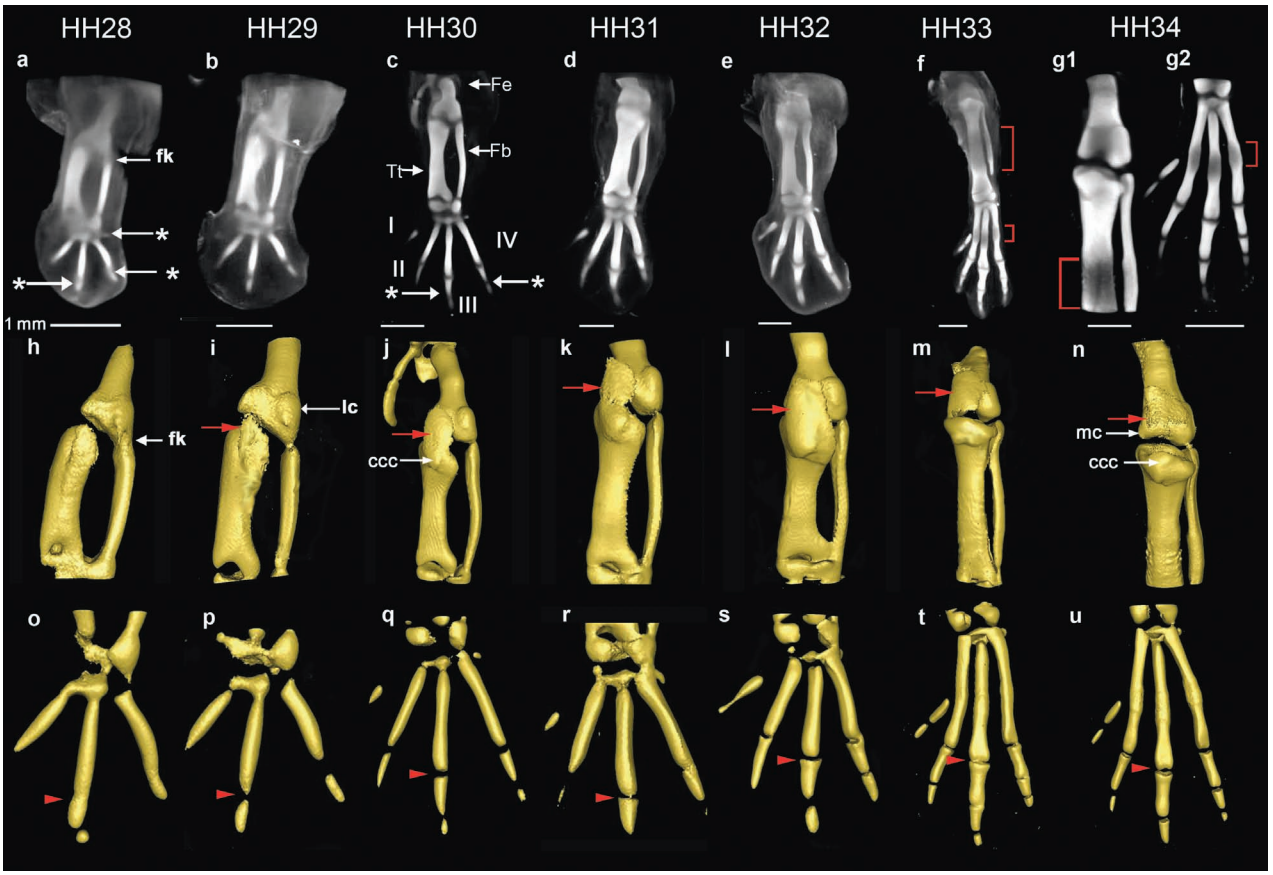

Fig. 1 3D analysis of the developing cartilaginous skeleton of the chick hind limb across stages HH28–34 stained with Alcian blue. (a–g) Dorsal views of 3D reconstructions of the data following OPT scanning. Due to the increased size at HH34, the limb was scanned twice, focusing separately on the knee joint region (g1) and footplate (g2). Surface representations of cartilaginous elements across (h–n) the future knee joint, and (o–u) the footplate (digits I–IV, indicated in c). Hypertrophy at the mid diaphysis is delineated by a bracket (f,g1,g2). The red arrow indicates the capsular condensation. The arrowheads follow the metatarso-phalangeal joint of digit III across stages (o–u). * indicates ankle (in a), MTP (in a) and interphalangeal joints (in c). Fe, femur; Fb, fibula; Tt, tibiotarsus; fk, forming knee; ccc, cranial cnemial crest; lc, lateral condyle; mc, medial condyle. Scale bars (1 mm) relate to a–g.

Alcian blue staining within the presumptive joint (Fig. 3c1,c2)). A clear indication of the lateral condyle structure appeared at stage HH29 on the posterior side of the femur (Fig. 1i) and increased in size and complexity over successive stages. Protrusion of the medial condyle on the anterior side of the femur occurred slightly later, beginning at HH31 [obscured by the joint capsule in Fig. 1k,l,m; Fig. 1n, (mc)]. In contrast to the human, the femur of the chick knee articulates with both the fibula and the tibiotarsus, so that the lateral condyle of the femur articulates with the fibula and the medial condyle with the tibiotarsus. On the lower (distal) surface of the knee, the cranial cnemial crest was evident as a bulge on the dorsal side of the tibia [Fig 1j, (ccc)] from HH30 and was clearly visible by HH34 (Fig. 1n). This structure ultimately develops into the root of the patellar ligament on the tibiotarsus. Through continuous elaboration over the period of observation the knee region had developed several of the main structural characteristics of the adult joint, including prominent condyles of the femur and the cranial cnemial crest by HH34 (Fig. 2).

Other joints also undergo morphogenesis during this period with the MTP joint of digit III developing furthest toward the congruent joint surfaces of the adult (series of arrowheads in Fig. 1o–u). Once fully separated at HH30, both joint surfaces were initially concave (Fig. 1q) but as development progressed the proximal joint surface gradually acquired a more convex shape (HH31) (Fig. 1r) and by HH33 had begun to develop the classic bicondylar structure (Fig. 1t) of the MTP joint. At HH34 the distal surface of the joint had also begun to acquire a bicondylar structure (Fig. 1u).

The capsular condensation (Mitrovic, 1978) appeared at HH29 as strong Alcian blue stained tissue on the dorsal side of the joint region (arrow in Fig. 1i). It covered the medial condyle of the femur and was continuous with the dorsal side of the tibia from HH29 (Fig. 1i–l, not visible in m or n due to threshold selection to preferentially view the joint). By HH34 the strongest stained region in the capsular condensation was directly over the forming femoral condyles at the position of the future patella (Fig. 1n). Further analysis of the developing capsule and patella are presented below (collagen XI expression).

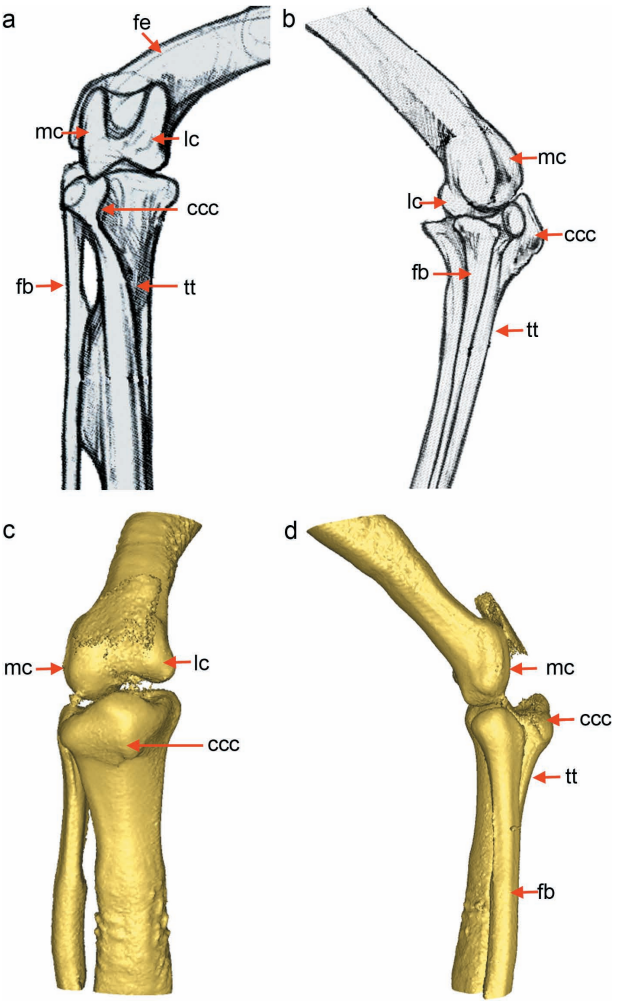

Fig. 2 Comparison of the adult galliform knee joint (Orosz et al. 1992) with the embryonic joint at HH34. By HH34 the embryonic joint (c–d) had the rudiments of several key structures seen in the adult (a–b). fe, femur; tt, tibiotarsus; fb, fibula; lc, lateral condyle; mc, medial condyle; ccc, cranial cnemial crest. Scale at HH34 as in Fig. 1.

The process of ossification began at HH32 as indicated by reduced levels of Alcian blue staining (due to cartilage hypertrophy) at the mid diaphysis of the femur (not shown) followed by similar patterns in the tibiotarsus, fibula and metatarsi at HH33 (Fig. 1f) and HH34 (Fig. 1g1,g2). Hypertrophy also leads to the bulges seen at the mid diaphysis of the long bones when viewed as surface representations, particularly in the digits at HH34 (Fig. 1u). Alizarin red staining confirmed that ossification was occurring in these regions (not shown).

Tissue subdivision within the joint interzone

While OPT analysis of Alcian blue staining captured the shape of the forming skeletal elements surrounding the joint line and showed a gradual reduction in Alcian blue staining within the forming interzone, the 3D analysis could not reveal the changes that occur at a cellular level. Therefore to integrate the detailed changes that occur in the cellular architecture during knee joint formation with the tissue level analysis of shape changes captured with OPT, paraffin wax sections through the knee joint region between stage HH28 and HH34 were stained with Alcian blue and haematoxylin. At HH28 the presumptive joint region or interzone could be identified as a region of increased cell density (8216 ± 161.8 cells mm^{-2} vs. 5200 ± 80.5 cells mm^{-2}) and decreased staining by Alcian blue (Fig. 3a1,a2). At each of the four stages the interzone had significantly greater cell density ($P < 0.001$) when compared to the surrounding cartilage (Fig. 3e). While the interzone was recognizably different from the surrounding cartilage, the continuous staining seen across the joint line explains the low definition of shape seen in the 3D reconstructions at early stages.

By HH30 cells within the interzone were oriented parallel to the articular surfaces (Fig. 3b2). These cells will ultimately form the articular cartilage, joint menisci and certain ligaments (Mitrovic, 1978; Ito & Kida, 2000). By HH32 the architecture of the interzone had changed again with the appearance of three layers (Fig. 3c1,c2). The two layers closest to the Alcian blue stained elements, the chondrogenous layers, are indicated by darker staining (Fig. 3c2) and separated by the intermediate layer. Ultimately the chondrogenous layers will form the articular cartilage and the joint menisci (Ito & Kida, 2000). The definition of the cartilaginous condensations (average cell density 3732 ± 73.9 cells mm^{-2}) was also clearer at HH32 (compare Fig. 3b2 and c2) with clear exclusion of Alcian blue staining from the interzone (cell density 6396 ± 213.7 cells mm^{-2}).

By HH34 the process of cavitation has commenced (Fig. 3d1,d2) with a cavity between the femur and fibula. A bifurcation in the forming cavity (Fig. 3d2) leads to the formation of the triangular tissue of the menisci (Fig. 3d2 indicated by m) that act to cushion the opposing surfaces from impact caused by movement. The process of sectioning can lead to some enlargement of acellular spaces such as the cavity. This is indicated by the normally smooth cavity walls (Fig. 3d2, arrowhead) appearing jagged with cells spanning the gap (Fig. 3d2, arrows). However, by sectioning multiple specimens and observing sections across the joint it was possible to verify the extent of real cavity formation.

Formation of the capsule

The expression pattern of the *α1 collagen type XI* gene (referred to as *Col XI* in the rest of this paper), a marker of connective tissue around the joint (Craig et al. 1987; Nalin et al. 1995), was analysed by *in situ* hybridization to characterize the size and shape of the capsular condensation. The joint capsule, patella and patellar ligaments are ultimately derived from this condensation. The capsular

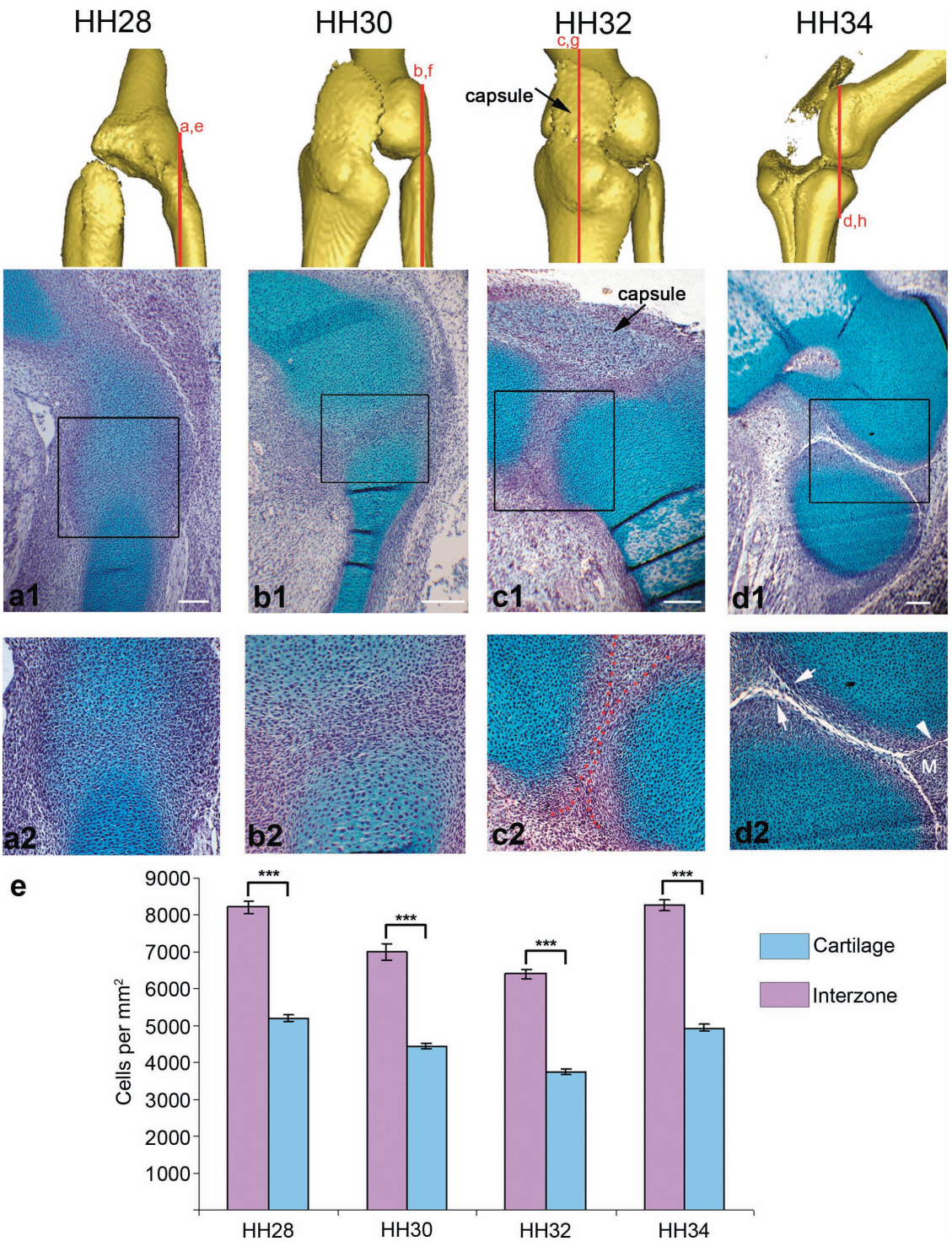

Fig. 3 Cellular changes in the forming knee joint between stages HH28 and HH34. Longitudinal sections through the chick knee joint (stages indicated above each column) at both low magnification (a1–d1) and high magnification (a2–d2) focusing on the interzone with the approximate plane of section represented by red lines above. All sections are presented with the femur lying above either the presumptive fibula (a,b,d) or tibia (c) (Note: no difference was seen in the cellular architecture described on the fibula or tibia side of the joint at HH32). Regions stained blue (Alcian blue) are cartilaginous, while the nuclear counterstain haematoxylin is purple. Red dotted lines (c2) indicate the boundary of the chondrogenous layers. (e) The cartilaginous regions had a significantly lower ($P \leq 0.001$) mean cell density than the intervening interzones at each stage (error bars represents SE) Arrowhead (d2) indicates joint cavity; arrows indicate artificially enlarged cavity; M, meniscus. Scale bars, 0.1 mm.

condensation was partially visible following Alcian blue staining (Fig. 1); however, *Col XI* expression gave a more complete representation of the extent of the forming structure. Examination of serial virtual sections in all orientations (representative sections only shown in Fig. 4) allowed the full extent of the capsular condensation to be defined at each stage. Initially the structure was seen at HH28 as intense staining dorsal to the knee joint and connected to the tibiotarsus (Fig. 4a, i–iv). At this point it does not encapsulate the entire knee joint. The expressing tissue at the three subsequent stages, resembled a sheath connected to the tibiotarsus, extending over the dorsal side of the femur and ultimately connecting with the tendon of the femorotibialis (Fig. 4c–e, iii) mirroring the position of the Alcian blue stained capsular condensation presented in Fig. 1(i–n). The structure also wraps across the dorsal side of the knee, encapsulating the entire knee from the medial to the lateral side (Fig. 4b–e, iv). No expression was found on the ventral side of the knee. At HH30 and HH32 the expression of *Col XI* was continuous with its expression in the perichondrium of the tibiotarsus; however, as the latter expression decreased, the capsule was distinguishable as an isolated band of *Col XI*-positive tissue encapsulating the knee (Fig. 4e, iii).

In addition to the capsular condensation, Col XI is also expressed in other tissues. Collagens are important components of tendons (van der Rest & Garrone, 1991) and expression of *Col XI* was found in the tendons on both the dorsal and ventral aspects of the tibiotarsus and fibula from stages HH30 to HH34 (Fig. 4c–e, i,vi). This aspect of *Col XI* expression is similar to that of the *Scleraxis* gene described below (Fig. 5). *Col XI* was also expressed in the ectoderm of the limb throughout all the stages analysed.

At the earliest stage examined (HH28, Fig. 4a,b) the distribution of *Col XI* mRNA resembled the shape of the emerging cartilaginous condensations, strongest in the metatarsals of digits II–IV and in recently formed proximal phalanges of digits III and IV (Fig. 4b, ii). On whole-mount preparations at later stages the expression of *Col XI* was no longer detected throughout the condensations of the tibiotarsus, fibula or metatarsus, but was detected in the perichondrium and adjacent to joint surfaces (Fig. 4c–e, ii–vi). *In situ* hybridization to sections showed continued low-level expression within chondrocytes of the proximal elements (not shown). The strongest *Col XI* expression was again evident throughout the condensations of the most distal elements, e.g. the proximal phalanges, and the distal phalanges of digits II–IV (Fig. 4C, i,ii).

Formation of muscle blocks and tendon attachment sites

Because of the close anatomical register and interdependence of muscle and tendon development, both tissues are described together here. Muscle development was visualized using an anti-myosin antibody, and the pattern of tendon formation was followed through two markers: (1) by *in situ* hybridization to detect expression of *Scleraxis* and (2) by immunolocalization of tenascin (Kardon, 1998) allowing double labelling of muscle and tendon. As previously reported (Shellswell & Wolpert, 1977; Kardon, 1998), muscles and tendons developed in a linked temporo-spatial pattern with three distinct territories of cells appearing in the future thigh, shank and foot regions, each territory divided into ventral and dorsal groups flanking the forming cartilaginous elements (Fig. 5).

Already by stage HH30 there were well-formed thigh and shank muscle masses on both the dorsal and ventral side of the limb (Fig. 5b–d). It was also possible to see the beginning of a further dorso-ventral subdivision into superficial and deep muscles (Fig. 5d), although subdivision of the more distal shank masses was not as distinct (Fig. 5c,d). At this stage tendon precursor cells were found in the knee region between thigh and shank (Fig. 5a), as well as at the distal end of the limb in the ankle and foot region (Fig. 5a,b). However, apart from three separate rod-like primordia in the foot (Fig. 5a,b), individual ankle and foot tendons were not yet defined. This parallels muscle formation where the muscles of the shank and foot had yet to separate and be excluded from the intervening ankle space.

By HH32 the muscle masses of the thigh and shank were much more clearly defined (Fig. 5f,g), as were the tendons (Fig. 5e). Boundaries were clear between the thigh and shank with delineation of superficial and deep muscle masses (Fig. 5h). The process of separation of foot muscles from the shank was complete (Fig. 5f). At HH32 it was possible to locate three separate territories of tendon primordia for the knee, ankle and foot (Fig. 5e) with tendons of the thigh and shank much more tightly defined (compare Fig. 5a and e). Some tendon attachment points could now be localized on the skeletal rudiments in the knee region, for example on the lower surface of the tibia (Fig. 5h); this tendon connects with the ilio-tibialis cranialis muscle. Although at HH32 the tendons of the foot had become better defined (Fig. 5e,f), expression remained relatively broad when compared with later stages (compare Fig. 5e and i).

The development of individual muscle masses was complete by HH34 with clear boundaries between muscles particularly in the thigh and shank (Fig. 5j–l). At this stage the full complement of muscles of the foot were visible as four individual blocks on both the dorsal and ventral aspect of the limb (Fig. 5j). This stage also showed the emergence of the complete set of limb tendons. The highly localized expression of both markers is particularly visible in the elongated tendons of the foot (Fig. 5i,j). Throughout the stages examined, it was interesting to note that localization of both tendon markers correlated with part of the collagen XI expression pattern in connective tissue (Fig. 4).

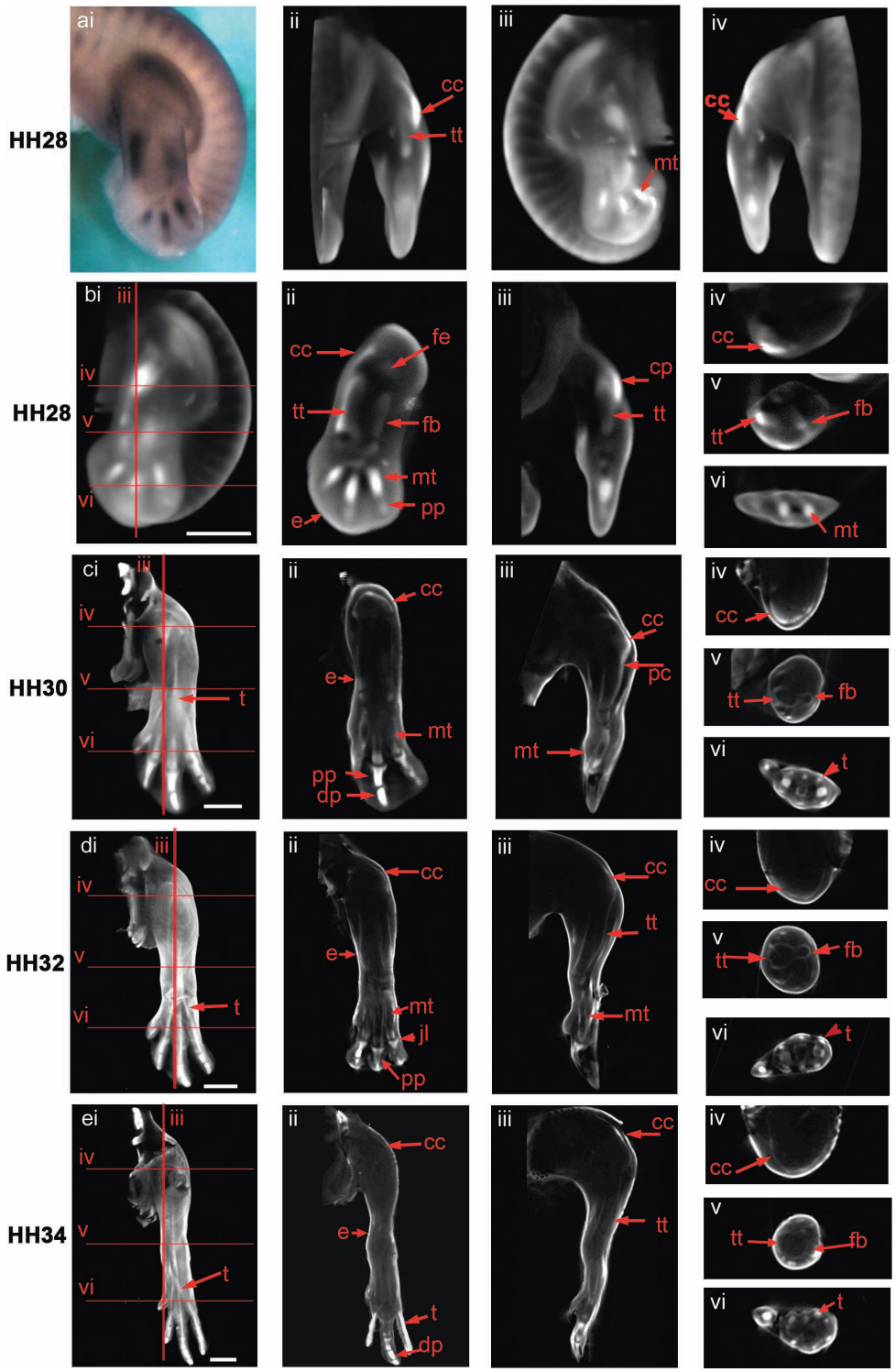

Fig. 4 Expression of the *Col XI* gene in the chick hind limb at stages HH28 (a,b), HH30 (c), HH32 (d), HH34 (e). ai shows a dorsal view of a stage HH28 limb prior to scanning. External views of a volume representation of the same limb following OPT scanning and reconstruction are shown in aii (rotated 90°), aiii (rotated 180°) and aiv (rotated 270°). b–d (i) show similar external dorsal views of whole reconstructed limbs with red lines indicating the plane of virtual longitudinal (iii) and transverse (iv–vi) sections taken through the 3D reconstructions. Sections shown in b, c and d ii were taken parallel to the view shown in i. Expressing tissue appears as white/light grey in the reconstructions (noted in the joint capsule, early condensing cartilage, the perichondria and epiphyses of more mature condensations and connective tissues). cc, capsular condensation; pc, perichondrium; pp, proximal phalange; dp, distal phalange; fb, fibula; fe, femur; mt, metatarsal; tt, tibiotarsus; t, tendon; jl, joint line. Scale bar, 1 mm.

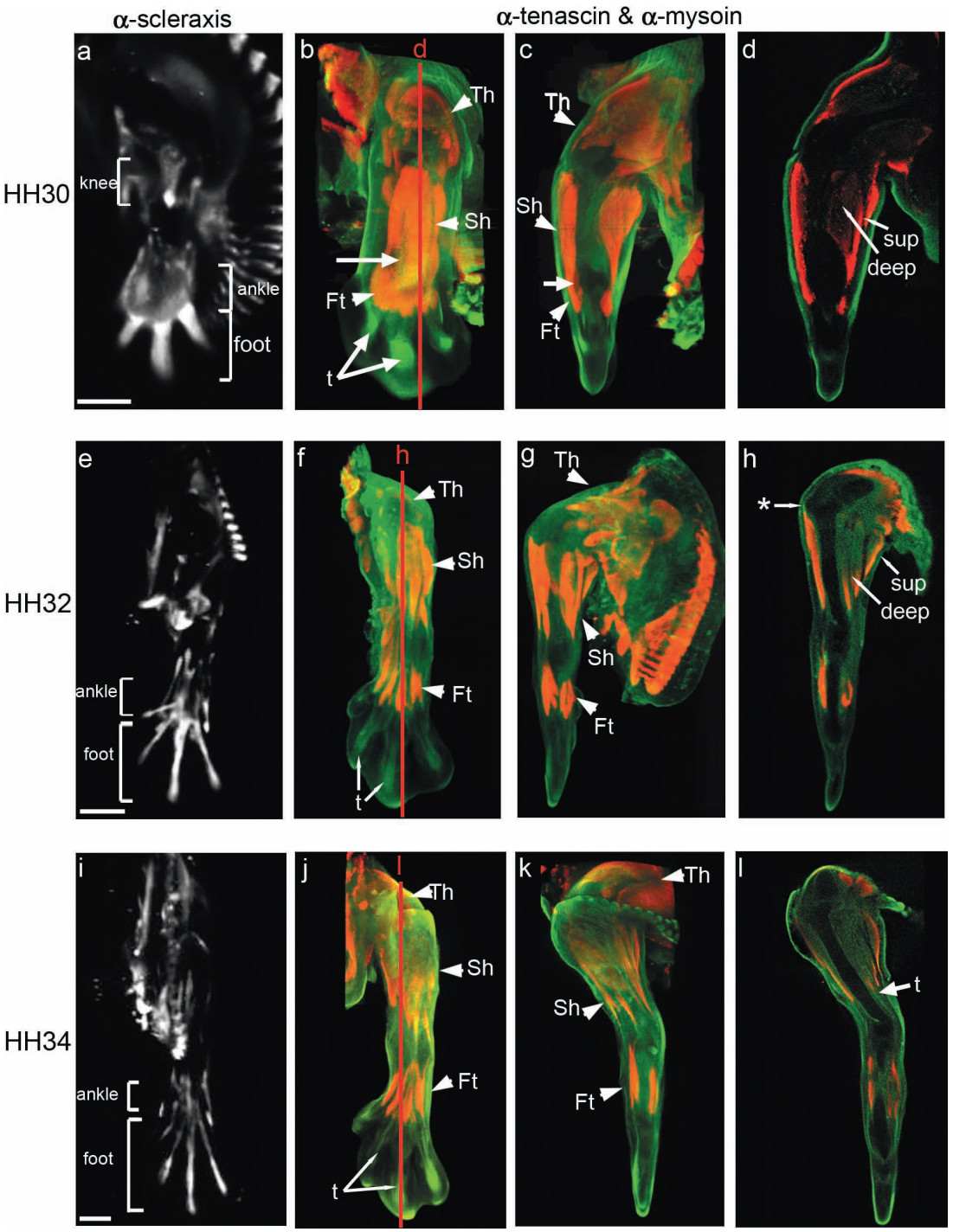

Fig. 5 Development of the muscle and tendon system in the chick hind limb at stages HH30, HH32 and HH34. The left column shows limbs viewed from the dorsal aspect from whole 3D reconstructions showing the localization of *Scleraxis* transcripts (a,e,i) (in white). Remaining images show double labelled specimens using α-tenascin (green) and α-myosin (red) antibodies. The second and third columns show external views of whole specimens (dorsal, b,f,j; anterior, c,g,k). d, h and l are longitudinal sections indicated by red lines. Territories of knee, ankle and foot tendons are delimited by brackets. Th, thigh muscles; Sh, shank muscles; Ft, foot muscles; sup, superficial muscles; deep, deep muscles; t, tendons. * indicates the ilio-tibialis cranialis tendon. Arrow in c indicates residual connections between muscle blocks. Scale bars, 1 mm.

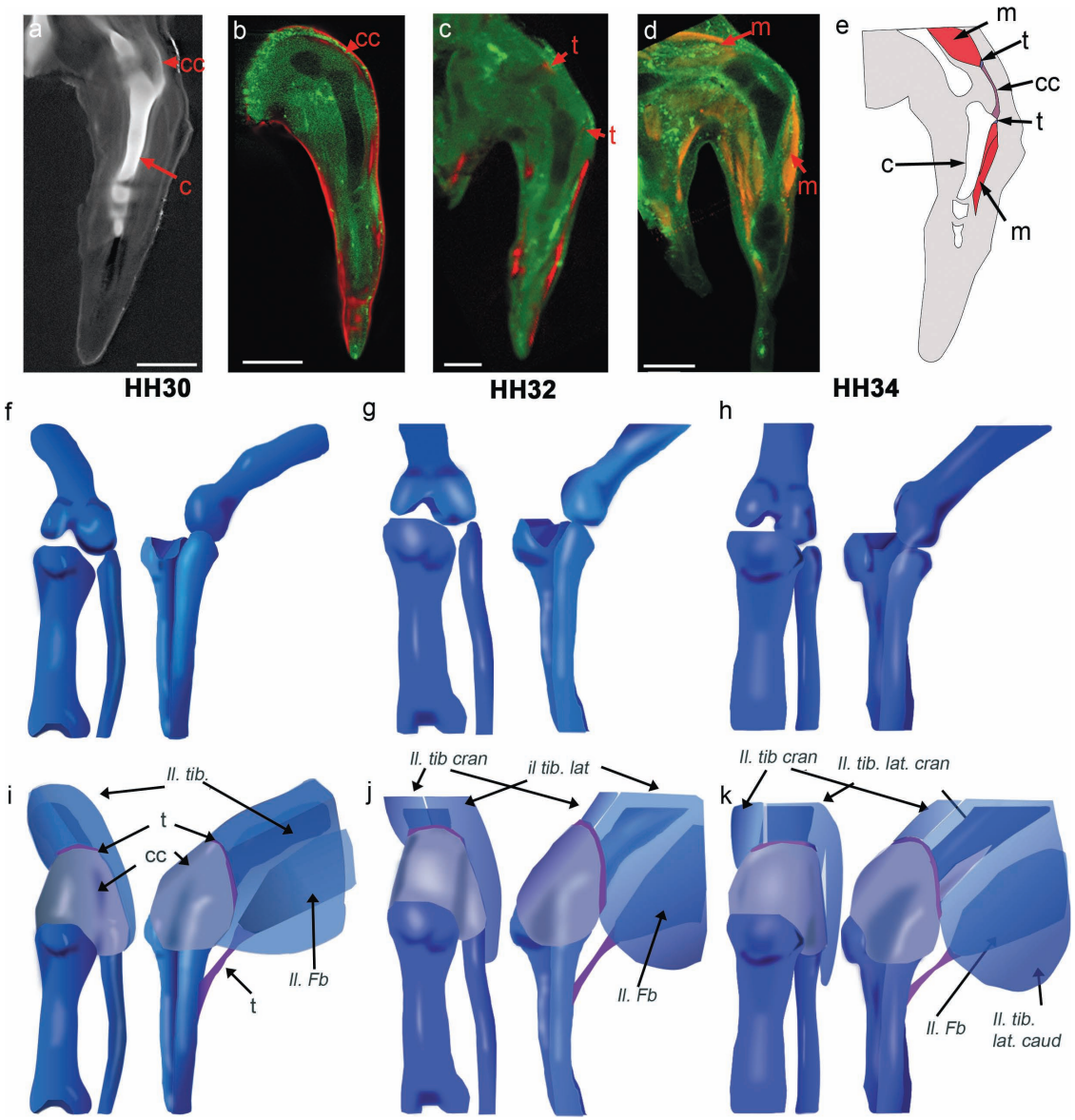

Fig. 6 Building 3D representations of the chick knee joint at stages HH30, HH32 and HH34, incorporating multiple components. Specimens stained with Alcian blue (Fig. 6a) give the shape of the cartilaginous elements (Fig. 6e–h). a–d show sample comparable longitudinal sections through the mid tibiotarsus (HH32) of specimens stained with Alcian blue (a), *in situ* hybridized for *Col XI* (b, pseudocoloured in red) *Scleraxis* (c, pseudocoloured in red) and immunostained to reveal myosin (d). e shows integration of the data. For 3D representation of the integrated data, the developing cartilage anlagen (e–g) (Fig. 1) firms the base onto which the shape of the capsule, the various tendon attachment sites and associated muscles were added (full complement of tendons and muscle not shown) (i–k). Muscles (nomenclature as per Baumel et al (1979)): *Il. Ti.*, ilio-tibialis (pre division into *Il. tib. lat* and *Il. tib. cran*); *Il. tib. lat.* (*caud/cran*), ilio-tibialis lateralis (caudalis/cranialis); *Il. tib. cran*., ilio-tibialis cranialis; *Il. Fb*., ilio-fibularis. c, cartilage; cc, capsular condensation; t, tendon; m, muscle. Scale bar, 1 mm.

Integrating the structural components

To represent the emerging spatial relationship between cartilage, capsule, tendon and muscle in the region of the knee joint, the individual components have been integrated in 3D representations of the emerging shape of the knee joint (Fig. 6; HH30, 32 and 34, Fig 1). Using virtual serial sections through 3D reconstructions of tendon visualization (both single and double labelling with muscle), individual tendons or precursor regions were correlated with the appropriate muscle blocks in the thigh and shank and placed on 3D representations of the cartilaginous elements (illustrated in Fig. 6). Figure 6a–e shows comparable views of cartilage, capsule, muscle and tendon data at HH34 illustrating the placement of the femoro-tibialis and peroneus tendon within the context of the other major components (Fig. 6e). The capsule was positioned in a similar manner with 3D representations in Fig. 6f–k

Table 2 Summary of the timing of key events observed during development of the knee joint and associated structures

	HH28	HH30	HH32	HH34
Cartilage				
Knee region	Position of future knee joint discernible *indication of lateral condyle of femur at HH29	Initial protrusion of future cranial cnemial crest	Appearance of medial condyle of femur apparent	Mature 3D shape of knee joint
Other joints	1st appearance of MTP joint of 3rd digit	Appearance of IP joint in digits III & IV, MTP joint of digit II. condensation of digit I	Appearance of 1st joint in digit 1	Bicondylar surface on MTP, joint digit 3
Bone			Ossification of femur	
Cavity formation	Interzone identified as region with higher cell density	Cells within interzone are orientated parallel to joint surface	3 layers at forming interzone	Cavity formation underway
Capsule (*α1 ColXI*)	Expression localized to condensing anlagen (similar to Alcian blue at this stage)	Encapsulates knee from the cranial cnemial crest to the dorsal thigh muscle masses	*α1 ColXI* expression is increasingly localized,forming a thin membrane surrounding joint	
Muscle		Separation of thigh and shank masses. Indication of further subdivision in thigh	Separation of foot from shank. Separation of muscle blocks in thigh	Full complement of thigh muscle blocks
Tendon		Broad expression in the 3 regions (knee, ankle, foot), 3 structures in digital region	Localization to presumptive tendons proximally with broader pattern in the foot	Well-defined tendons

showing the placement of the capsule and several tendon attachment sites. Two of the principal muscles of the thigh are illustrated: the ilio-tibialis, prior to and after it splits into the lateralis and cranialis blocks (Fig. 6i,j), which attaches to the joint capsule; and the ilio-fibularis where it attaches to the fibula. Other muscle blocks whose associated tendons were placed but not illustrated include the femoro-tibialis muscle, located on the dorsal side of the femur under the ilio-tibialis, which attaches to the joint capsule, and the ventral flexor cruris and pubo-ischo-femoralis muscles, which attach to the tibiotarsus and femur, respectively (nomenclature as per Baumel et al. 1979). While only the thigh muscles have been indicated, other muscles including ventral and dorsal shank muscles and the muscles of the foot were also tracked to their associated myotendinous junction and onto their associated cartilage.

Discussion

We have built 3D representations of the developing knee joint in the chick incorporating morphological changes in the developing cartilage, muscle, tendon, joint capsule and synovial cavity in an integrated model. We show that the cartilage rudiments in the chick limb acquire the shape characteristics of the adult knee joint early in development, at stage HH34. Such an appreciation of detailed shape acquisition was not previously possible from viewing 2D images of Alcian blue stained preparations or histological sections. By capturing the process of joint formation in 3D it was possible to gather more detailed and sophisticated temporo-spatial information about the emergence of joint shape and the appearance and inter-relationship of multiple associated tissues such as muscles, tendons, the joint cavity and capsule, and to integrate the different strands of information in a 3D representation of the events. In addition to recording and describing events in 3D, the relative timing was also recorded focusing on a single joint (Table 2).

Analysing and representing the joint structure in 3D provides a realistic frame of reference for normal development and can be used for example in the generation of morphologically realistic computational models (Nowlan et al. 2008). 3D joint representation can also be extended with additional information such as the distribution of regulatory molecules at key stages and could also form the basis for comparison of pathological joint development in genetically or physically altered laboratory situations. Although 3D representations can be reconstructed from serial 2D images the process is time-consuming and fraught with issues of filling in gaps in the data and distortions resulting from alignment of individual 2D sections (discussed in Hecksher-Sørensen & Sharpe, 2001). Direct 3D capture

of the data was facilitated by using OPT imaging (Sharpe, 2003). While other approaches could in principle capture part of the data in 3D (MRI for morphology and confocal microscopy to view fluorescent markers in thick sections), OPT is the only technique that can image morphology, colourimetric stains such as those commonly used for gene expression analysis and histology, and fluorescent markers, in whole embryonic limbs. Most previous descriptions of the developing knee joint have been put together from 2D data (Murray & Drachman, 1969; Mitrovic, 1977; Persson, 1983) or partial 3D confocal data, such as the elegant study by Kardon (1998) on the morphogenesis of muscle and tendon. The current work is the first 3D representation of knee joint morphogenesis including information assembled on different components of the system, as illustrated in Fig. 6.

The first step of this process was the representation of the changing shape of the cartilaginous condensations around the forming joint stained with Alcian blue (Figs 1 and 6f–h). We found that the knee joint region undergoes the most dramatic shape changes between HH30 and HH34 with the outgrowth of the condyles of the femur as well as the cranial cnemial crest. At HH30 the joint has just begun to acquire structure with the outgrowth of the lateral condyle, and consecutive stages illustrate the emergence of the medial condyle as well as the cranial cnemial crest, so that by HH34 the femur has acquired a complex 3D bicondylar structure and the dorsal surface of the tibia has developed a pronounced protrusion (cranial cnemial crest). The capsule and ligaments provide structural support to the developing joint and are another important component of the system to be included in any integrated representation. At the stages investigated here the ligaments of the knee including the cruciate and lateral ligaments have not yet formed (Kardon, 1998; Schweitzer et al. 2001); however, the capsular condensation, a structure which ultimately gives rise to the patella, joint capsule, patellar tendons and ligaments (Bland & Ashhurst, 1997), has begun to emerge. The capsular condensation, visualized using the capsule marker Col XI (Nalin et al. 1995), was located on the dorsal side of the tibia at all three stages, extending from the tibiotarsus over the dorsal side of the knee and its position and size is represented in Fig. 6. Ultimately this structure connects with the tendon of the ilio-tibialis and femoro-tibialis muscles.

Muscle contractions have been identified as an important influence on joint cavity formation (Drachman & Sokoloff, 1966; Murray & Drachman, 1969; Persson, 1983; Osborne et al. 2002; Bastow et al. 2005; Kavanagh et al. 2006) and determining exactly when muscle blocks and tendons appear and form functional connections to the forming cartilage is an important aspect of understanding events as cavitation occurs. Prior to HH30, some indications of the muscles and tendons of the future thigh, shank and foot were visible (Fig. 5a,c). As development proceeded, the muscle and tendon masses underwent subdivision, ultimately leading to the formation of the full adult complement by HH34. As the aim of this work was not just to characterize the development of structures individually but also to generate an integrated representation, the placement of tendon attachments around the joint was a key goal. This was particularly challenging because the muscle and tendon systems consist of numerous individual elements which spatially overlap each other and, despite the use of specific markers and 3D imaging, were difficult to trace individually and match in separate specimens. However, double labelling of tendons and muscles in the same specimens enabled the tracking of individual muscle masses directly to their associated tendons and onto their cartilaginous attachments. By combining the information from both the *Scleraxis in situ* and the α-tenascin and α-myosin immunohistochemistry, it was possible to determine the 3D relationship between the principal elements of the musculoskeletal system.

OPT analysis of histological and gene expression data allows detailed 3D visualization at the tissue level. However, this approach does not allow an investigation of changes at a cellular level given the current limit to the resolution of the technique (Sharpe et al. 2002). To answer certain specific questions it is necessary to combine data from other approaches. Visualization of Alcian blue staining of the cartilaginous elements showed a clear reduction in staining intensity in the forming joint region across the time period but it was difficult to determine what changes were occurring in the interzone including when the forming skeletal elements were ultimately separated and when a cavity appeared. To investigate the development of the interzone, histological sections were prepared and showed a gradual disappearance in Alcian blue staining and a concomitant increase in the definition of the skeletal elements with clear delineation at HH30. At the same time the cells of the interzone showed a higher cell density and underwent a change in cell orientation (HH30) with the appearance of the three layers of the interzone (Ito & Kida, 2000) at HH32 and the first appearance of a cavity at HH34. While this data is not 3D it provides vital information about the nature of the interzone and its surrounding tissues and the process of forming the joint cavity. This provides important additional information for computational modelling of the system and comparison to manipulated situations.

An important result of this study was the elucidation of the co-ordinated timing of individual events within the chick limb. Table 2 summarizes the main events in the emergence of the various components. For example HH29–30 sees elaboration of skeletal morphology with emergence of the lateral condyle (HH29) and cranial cnemial crest (HH30), while muscles and tendons of the thigh and shank have separated and undergone subdivision to form the superficial and deep muscle masses, and knee tendon primordia

appear in the space previously occupied by undivided muscle. Immobilization studies show that the knee joint is also most susceptible to alterations in mechanical stimuli during the period HH30–34 (Drachman & Sokoloff, 1966). This indicates that the close temporal relationship between the emerging joint shape and muscle system is not coincidental but is the basis of a co-ordinated system where at least part of the information guiding joint shape comes from muscle activity. We now have a 3D temporal and spatial framework in which such inter-relationships can be explored computationally and experimentally.

Concluding remarks

This study is the first to characterize the formation of a joint structure in 3D and represents an increase in our understanding of joint shaping. In addition, the process of building this dataset could have wider applications for the study of complex multi-component structures in diverse organisms representing a new approach to investigating the factors that influence morphogenesis. We need to address morphogenesis at this integrated level because despite our more sophisticated view of the molecular regulation of developmental events, we still have a poor understanding of how the 3D shape of a forming tissue is defined.

The type of 3D analysis applied here to normal embryos could also be applied to embryos which have been experimentally manipulated by immobilization (Drachman & Sokoloff, 1966; Osborne et al. 2002; Kavanagh et al. 2006), surgery (Holder, 1977) or the introduction of ectopic regulatory factors (Merino et al. 1999), or embryos which have an inherent skeletal abnormality (such as Kwok et al. 1995; Poetter et al. 1996; Gong et al. 1999). This could in turn lead to a better understanding of how these abnormalities not only affect a component such as cartilage directly, but lead to associated alterations in other components. One possible use might be a more sophisticated analysis of the effects of immobilization to determine how alterations in the mechanical environment can lead not only to alterations in joint shape, but also the associated structures such as tendons, sesamoid bones such as the patella, and the joint cavity. Thus by understanding the interrelationships between multiple tissues in the developing structure it may be possible to understand morphogenesis as an integrated process involving numerous components within a network of intrinsic and extrinsic signals.

Acknowledgements

This work was supported by a studentship from Trinity College Dublin (SFI AOIP interdisciplinary program) and by Science Foundation Ireland (Programme Award 02/IN1/B267). We thank Ms Kristen Summerhurst, Dr Adrian Dervan and Mr Peter Stafford for technical advice.

References

Alanentalo T, Asayesh A, Morrison H, et al. (2007) Tomographic molecular imaging and 3D quantification within adult mouse organs. *Nat Methods* **4**, 31–33.

Asou Y, Nifuji A, Tsuji K, et al. (2002) Coordinated expression of *scleraxis* and *Sox9* genes during embryonic development of tendons and cartilage. *J Orthop Res* **20**, 827–833.

Bastow E, Lamb K, Lewthwaite J, et al. (2005) Selective activation of the MEK-ERK pathway is regulated by mechanical stimuli in forming joints and promotes pericellular matrix formation. *J Biol Chem* **280**, 11749–11758.

Baumel JJ, King A, Lucas A, Breazile JE, Evans EH (eds) (1979) *Nomina Anatomica Avium: An Annotated Anatomical Dictionary of Birds*. London: Academic Press.

Bellairs R, Osmond M (2005) *Atlas of Chick Development*. pp. 91–104. Oxford: Elsevier Academic Press.

Benjamin M, Ralphs JR (2000) The cell and developmental biology of tendons and ligaments. *Int Rev Cytol* **196**, 85–130.

Bi W, Deng JM, Zhang Z, Behringer RR, de Crombrugghe B (1999) Sox9 is required for cartilage formation. *Nat Genet* **22**, 85–89.

Bland YS, Ashhurst DE (1997) Fetal and postnatal development of the patella, patellar tendon and suprapatella in the rabbit; changes in the distribution of the fibrillar collagens. *J Anat* **190**(Pt 3), 327–42.

Boardman PE, Sanz-Ezquerro J, Overton IM, et al. (2002) A comprehensive collection of chicken cDNAs. *Curr Biol* **12**, 1965–1969.

Borello U, Berarducci B, Murphy P, et al. (2006) The Wnt/{beta}-catenin pathway regulates Gli-mediated Myf5 expression during somitogenesis. *Development* **133**, 3723–3732.

Buckingham M, Bajard L, Chang T, et al. (2003) The formation of skeletal muscle: from somite to limb. *J Anat* **202**, 59–68.

Chenna R, Sugawara H, Koike T, et al. (2003) Multiple sequence alignment with the Clustal series of programs. *Nucleic Acids Res* **31**, 3497–500.

Craig FM, Bentley G, Archer CW (1987) The spatial and temporal pattern of collagens I and II and keratan sulphate in the developing chick metatarsophalangeal joint. *Development* **99**, 383–391.

Cserjesi P, Brown D, Ligon KL, et al. (1995) Scleraxis: a basic helix-loop-helix protein that prefigures skeletal formation during mouse embryogenesis. *Development* **121**, 1099–1110.

DeLaurier A, Schweitzer R, Logan M (2006) Pitx1 determines the morphology of muscle, tendon, and bones of the hindlimb. *Dev Biol* **299**, 22–34.

Drachman DB, Sokoloff L (1966) The role of movement in embryonic joint development. *Dev Biol* **14**, 401–420.

Eyre D (2002) Collagen of articular cartilage. *Arthritis Res* **4**, 30–35.

Fell HB (1925) The histogenesis of cartilage and bone in the long bones of the embryonic fowl. *J Morphol* **40**, 417–459.

Garciadiego-Cazares D, Rosales C, Katoh M, Chimal-Monroy J (2004) Coordination of chondrocyte differentiation and joint formation by alpha5beta1 integrin in the developing appendicular skeleton. *Development* **131**, 4735–4742.

Gelse K, Poschl E, Aigner T (2003) Collagens – structure, function, and biosynthesis. *Adv Drug Deliv Rev* **55**, 1531–1546.

Gong Y, Krakow D, Marcelino J, et al. (1999) Heterozygous mutations in the gene encoding noggin affect human joint morphogenesis. *Nat Genet* **21**, 302–304.

Hamburger V, Hamilton HL (1951) A series of normal stages in the development of the chick embryo. *J Morphol* **88**, 49–92. Republished (1992) *Developmental Dynamics* **195**, 231–272.

Hartmann C, Tabin CJ (2000) Dual roles of Wnt signaling during chondrogenesis in the chicken limb. *Development* **127**, 3141–3159.

Hecksher-Sørensen J, Sharpe J (2001) 3D confocal reconstruction of gene expression in mouse. *Mech Dev* **100**, 59–63.

Hogan B, Beddington R, Costantini F, Lacy E (1994) *Manipulating the Mouse Embryo: A Laboratory Manual*. Cold Spring Harbor, NY: Cold Spring Harbor Laboratory.

Holder N (1977) An experimental investigation into the early development of the chick elbow joint. *J Embryol Exp Morphol* **39**, 115–127.

Ito MM, Kida MY (2000) Morphological and biochemical re-evaluation of the process of cavitation in the rat knee joint: cellular and cell strata alterations in the interzone. *J Anat* **197**(Pt 4), 659–679.

Kardon G (1998) Muscle and tendon morphogenesis in the avian hind limb. *Development* **125**, 4019–4032.

Kavanagh E, Church VL, Osborne AC, et al. (2006) Differential regulation of GDF-5 and FGF-2/4 by immobilisation in ovo exposes distinct roles in joint formation. *Dev Dyn* **235**, 826–834.

Kerwin J, Scott M, Sharpe J, et al. (2004) 3 dimensional modelling of early human brain development using optical projection tomography. *BMC Neurosci* **5**, 27.

Kwok C, Weller PA, Guioli S, et al. (1995) Mutations in SOX9, the gene responsible for Campomelic dysplasia and autosomal sex reversal. *Am J Hum Genet* **57**, 1028–1036.

Lee K, Avondo J, Morrison H, et al. (2006) Visualizing plant development and gene expression in three dimensions using optical projection tomography. *Plant Cell* **18**, 2145–2156.

Lelkes G (1958) Experiments in vitro on the role of movement in the development of joints. *J Embryol Exp Morphol* **6**, 183–186.

Lioubinski O, Alonso MT, Alvarez Y, et al. (2006) FGF signalling controls expression of vomeronasal receptors during embryogenesis. *Mech Dev* **123**, 17–23.

Merino R, Macias D, Ganan Y, et al. (1999) Expression and function of Gdf-5 during digit skeletogenesis in the embryonic chick leg bud. *Dev Biol* **206**, 33–45.

Miller SFC, Summerhurst K, Runker AE, et al. (2007) Expression of Plxdc2/TEM7R in the developing nervous system of the mouse. *Gene Expr Patterns* **7**, 635–644.

Mitrovic DR (1977) Development of the metatarsophalangeal joint of the chick embryo: morphological, ultrastructural and histochemical studies. *Am J Anat* **150**, 333–347.

Mitrovic DR (1978) Development of the diarthrodial joints in the rat embryo. *Am J Anat* **151**, 475–485.

Murray PD, Drachman DB (1969) The role of movement in the development of joints and related structures: the head and neck in the chick embryo. *J Embryol Exp Morphol* **22**, 349–371.

Nalin AM, Greenlee TK Jr, Sandell LJ (1995) Collagen gene expression during development of avian synovial joints: transient expression of types II and XI collagen genes in the joint capsule. *Dev Dyn* **203**, 352–362.

Nowlan NC, Murphy P, Prendergast PJ (2008) A dynamic pattern of mechanical stimulation promotes ossification in avian embryonic long bones. *J Biomech* **41**, 249–258.

Orosz SE, Ensley PK, Haynes CJ (1992) *Avian Surgical Anatomy: Thoracic and Pelvic Limbs*. Philadelphia: W.B. Saunders.

Osborne AC, Lamb KJ, Lewthwaite JC, Dowthwaite GP, Pitsillides AA (2002) Short-term rigid and flaccid paralyses diminish growth of embryonic chick limbs and abrogate joint cavity formation but differentially preserve pre-cavitated joints. *J Musculoskelet Neuronal Interact* **2**, 448–456.

Persson M (1983) The role of movements in the development of sutural and diarthrodial joints tested by long-term paralysis of chick embryos. *J Anat* **137**(Pt 3), 591–599.

Poetter K, Jiang H, Hassanzadeh S, et al. (1996) Mutations in either the essential or regulatory light chains of myosin are associated with a rare myopathy in human heart and skeletal muscle. *Nat Genet* **13**, 63–69.

Rodriguez JI, Garcia-Alix A, Palacios J, Paniagua R (1988) Changes in the long bones due to fetal immobility caused by neuromuscular disease. A radiographic and histological study. *J Bone Joint Surg Am* **70**, 1052–1060.

Sarma S, Kerwin J, Puelles L, et al. (2005) 3D modelling, gene expression mapping and post-mapping image analysis in the developing human brain. *Brain Res Bull* **66**, 449–453.

Schweitzer R, Chyung JH, Murtaugh LC, et al. (2001) Analysis of the tendon cell fate using Scleraxis, a specific marker for tendons and ligaments. *Development* **128**, 3855–3866.

Sharpe J (2003) Optical projection tomography as a new tool for studying embryo anatomy. *J Anat* **202**, 175–181.

Sharpe J, Ahlgren U, Perry P, et al. (2002) Optical projection tomography as a tool for 3D microscopy and gene expression studies. *Science* **296**, 541–545.

Shellswell GB, Wolpert L (1977) The pattern of muscle and tendon development in the chick wing. In *Vertebrate Limb and Somite Morphogenesis* (eds Ede DA, Hincliffe JR, Balls M), pp. 71–86. Cambridge: Cambridge University Press.

Summerhurst K, Stark M, Sharpe J, Davidson D, Murphy P (2008) 3D representation of Wnt and Frizzled gene expression patterns in the mouse embryo at embryonic day 11.5 (Ts19). *Gene Expr Pattern* doi:101016/jgep200801007.

van der Rest M, Garrone R (1991) Collagen family of proteins. *FASEB J* **5**, 2814–2823.

Xu Q, Wilkinson D (1998) In situ hybridisation of mRNA with hapten labelled probes. In *In Situ Hybridisation: A Practical Approach* (ed. Wilkinson DG), pp. 87–106. Oxford: Oxford University Press.